Zhang *et al.*
Chinese Journal of Mechanical Engineering (2022) 35:141
https://doi.org/10.1186/s10033-022-00811-3

Chinese Journal of Mechanical Engineering

ORIGINAL ARTICLE

Open Access

Design of Passive Constant-Force End-Effector for Robotic Polishing of Optical Reflective Mirrors

Jian Zhang[1,2], Liangxiao Zhao[2,3], Lingling Li[4], Fulei Ma[1] and Guimin Chen[4*]

Abstract

Polishing plays an indispensable role in optical processing, especially for large-aperture optical reflective mirrors with freeform surfaces. Robotic polishing requires effective control of the contact force between the robot and the mirror during processing. In order to maintain a constant contact force during polishing, traditional polishing robots rely on closed-loop control of air cylinders, whose performances heavily rely on high-fidelity force sensing and real-time control. This paper proposes to employ a compliant constant-force mechanism in the end-effector of a polishing robot to passively maintain a constant force between the robot and the mirror, thus eliminating the requirement for force sensing and closed-loop control. The compliant constant force mechanism utilizing the second bending mode of fixed-guided compliant beams is adopted and elaborated for the passive end-effector. An end-effector providing a constant contact force of 40 N is designed and prototyped. The polishing experiment shows that the passive constant-force end-effector provides stable contact force between the robot and the mirror with fluctuation within 3.43 N, and achieves RMS (Root Mean Square) lower than λ/10 (λ = 632.8 nm) of the polished surface of the large-aperture optical reflective mirror. It is concluded that the constant-force compliant mechanism provides a low-cost and reliable solution for force control in robotic polishing.

Keywords: Robotic polishing, Fixed-guided compliant beam, Constant-force compliant mechanism, Passive force control

1 Introduction

With the development of space optical communication and remote imaging, the demand for large-aperture optical components is increasing. Polishing plays an indispensable role in optical processing, especially for large-aperture optical reflective mirrors with freeform surfaces [1, 2]. Under this circumstance, traditional grinding and polishing technologies are no longer efficient. The demands for low-cost and high-efficiency polishing robots have become much more substantial. The existing polishing robots combine industrial robots with a constant force polishing end effector [3]. The industrial robotic arm adjusts its end position and orientation according to the irregular shape of the workpiece to be polished. Moreover, the end effector applies a constant polishing force to the workpiece to ensure surface quality and polishing efficiency. Therefore, the performance of the end effector directly determines the polishing performance of the robot.

Currently, the end effector realizes its constant force mainly by means of active force control, which requires high-fidelity force sensors and complicated control strategies [4]. Two main ways, including air cylinder and voice coil motor, are commonly used to obtain constant force property. Force feedback as well as specific control strategies was used to control the force execution unit, such as adjusting air pressure and electric current. Moriyasu

*Correspondence: guimin.chen@xjtu.edu.cn

[4] Institute of Robotics and Intelligent Systems, Xi'an Jiaotong University, Xi'an 710049, China
Full list of author information is available at the end of the article

et al. [5] used a low friction air cylinder to polish aspheric surfaces. The force/position control was used to achieve high-quality control of the air cylinder. Su et al. [6] introduced a buffer cylinder which further improved the accuracy of the constant force control of the cylinder. Monhammad et al. [7] proposed an end-effector utilizing a voice coil motor, which tunes the polishing through a PID controller based on the feedback of a force sensor. Furthermore, they used the high responsiveness of the voice coil motor to complete the surface error leveling of the metal parts.

The aforementioned solutions used active force control methods to realize constant contact force. They all utilize complex controllers and high-fidelity force sensors [8] to achieve required performances. However, this work proposes to achieve constant-force through a passive way. To be more specific, we designed a constant-force compliant mechanism, which is used it as the end effector of the polishing robot to maintain a constant-force for high-precision optical polishing.

A compliant constant-force mechanism (CCFM), which can provide a near-constant force output over a displacement range [9], shows promise for passive constant-force control. The advantages of compliant mechanisms include fewer parts, easier to be manufactured and no need to be lubricated [10]. Furthermore, it is easier to be integrated in the system than the above two end-effectors with force-feedback control. Chen and Lan [11] designed a CCFM for robotic end-effectors by combining negative stiffness of a bistable mechanism and positive stiffness of a linear spring. Chen and Zhang [12] presented a new idea of obtaining constant-force behaviors through combining two multistable compliant mechanisms [13]. Kuo and Lan [14] presented a novel constant-force mechanism that can produce adjustable constant force in two dimensions. Ma and Chen [15] proposed a CCFM utilizing the second bending mode of fixed-guided compliant beams, which realizes a large-stroke constant behavior with a relatively simple structure.

In this work, the CCFM proposed by Ma and Chen [16] is adapted and tailored for the passive compliant constant-force polishing end-effector for the purpose of optical component fabrication, as shown in Figure 1. Section 2 provides the design of the CCFM and the constant-force behavior is verified by a kinetostatic model based on the chained beam constraint model (CBCM). The detailed structure design of the constant-force end-effector is given in Section 3; Section 4 contains comprehensive performance experiments and polishing experiments to verify the effectiveness of the compliant constant-force polishing end-effector; The conclusions and future work are discussed in Section 5.

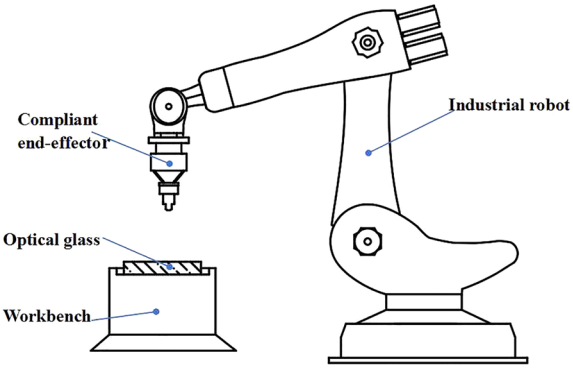

Figure 1 Diagram of polishing robot

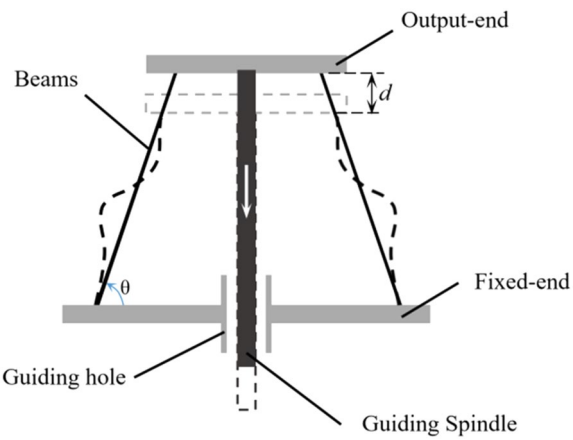

Figure 2 Constant-force mechanisms

2 Design of Constant-Force Compliant Mechanism

Figure 2 shows the schematic of the constant-force compliant mechanism that is used in the polishing end effector. Each of the flexible beams is fixed on one end while guided on the other end with unchanged tip angle. A guiding spindle is used in the mechanism to increase its bending stiffness. Since the beams undergo large deflections, CBCM [17] is used to characterize their load-deflection behaviors.

2.1 Parametric Design

When designing a constant force mechanism utilizing the buckling characteristics of flexible beams, two performance metrics should be considered. One metric is the variation of the output force ξ (magnitude of constant force fluctuation), which is defined as:

$$\xi = \max\left(\frac{|F - F_N|}{F_N}\right), \tag{1}$$

where F is the actual output force of the mechanism at any position in the operational displacement range and F_N is the desired output force. The other metric is the operational displacement range S, which is defined as a continuous flatten part of the force-displacement curve. Detailed definitions of the two performance metrics can be found in our previous work [16].

The current study aims at designing a constant force mechanism for polishing large-aperture reflective mirrors with freeform surfaces. Generally, the contact force needs to be strictly controlled, which should be no more than 50 N (for thin and brittle lenses, the contact force needs to be further reduced). Thus, we set the target contact force as 40 N. According to the structure of the constant force end-effector, the compliant constant force mechanism provides constant force output with 26 N, and the mechanical structure parts of the movable end of the end-effector provide constant force with 14 N. Moreover, the variation of the force fluctuation should not exceed 10%. For a typical polishing process, an operational displacement range of 10 mm is enough.

To meet the performance metrics given above, we can determine the design parameters of the constant force mechanism using the quick design formulas given in Ref. [16]. The problem is formulated as:

$$\max S(\theta), \tag{2}$$

subject to

$$\xi \le 0.1, 0 \le \beta \le \frac{\pi}{2}, \tag{3}$$

where ξ is the allowed variation of the output force.

Then, we get the curves of S/L (L is the beam length) versus β for $\xi = 10\%$, which is shown in Figure 3. To meet the requirement of operational displacement $S/L > 0.16$, we should choose the β in the range from 35° to 47°. As shown in Figure 3, multiple results meet the design requirements. Due to the compactness requirement of the entire structure, the following parameters are selected

$$\begin{aligned} S/L &= 0.2, \\ \beta &= 40^\circ. \end{aligned} \tag{4}$$

The nondimensionalized output force can be formulated as

$$\frac{12N_bF_NL^2}{EWT^3} = 40. \tag{5}$$

By rearranging the above equation, the thickness of the flexible beam can be expressed as

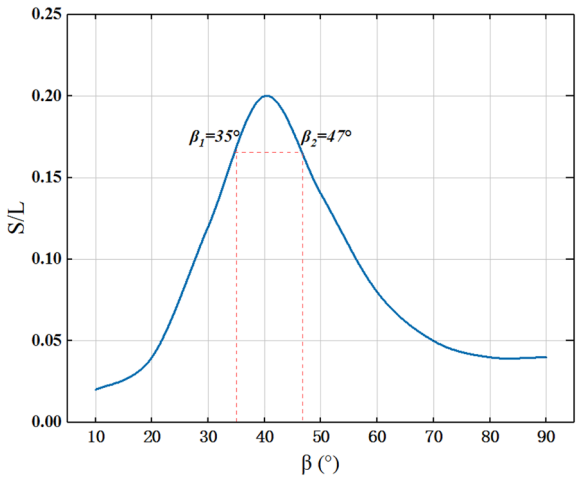

Figure 3 The S/L with respect to β

$$T = \left(\frac{F_NL^2}{3.03N_bEW}\right)^{1/3}. \tag{6}$$

The values of the design parameters are determined as: $N_b = 4$, $L = 60$ mm, $W = 5$ mm, $T = 0.2$ mm, and $\beta = 40°$.

2.2 Modeling

To further verify the feasibility of the design given in the last section, a kinetostatic model for the constant-force design is established. Due to the symmetry of the design, only one limb is selected to be modeled as a fixed-guided beam. Figure 4 shows discretization of the fixed-guided beam. The global coordinate frame xOy is established with its origin placed at the fixed end of the compliant beam (point A) and the positive direction of the x-axis along the length of the beam. We divide the fixed-guided compliant beam into N elements and model the beam using CBCM.

The parameters are defined as follows: L is the length of the compliant beam AB, W is the width, T is the thickness, E is the Young's modulus of the material, and I is the area moment of inertia ($I = WT^3/12$). When deflected, X_o, Y_o, and θ_o are used to represent the tip coordinates and the tip angle, respectively.

According to the boundary conditions, X_o and Y_o (the coordinates of the guided end) in Figure 4 can be expressed as:

$$X_o = L - d\sin\theta_o, \tag{7}$$

$$Y_o = (L - X_o)\tan\theta_o, \tag{8}$$

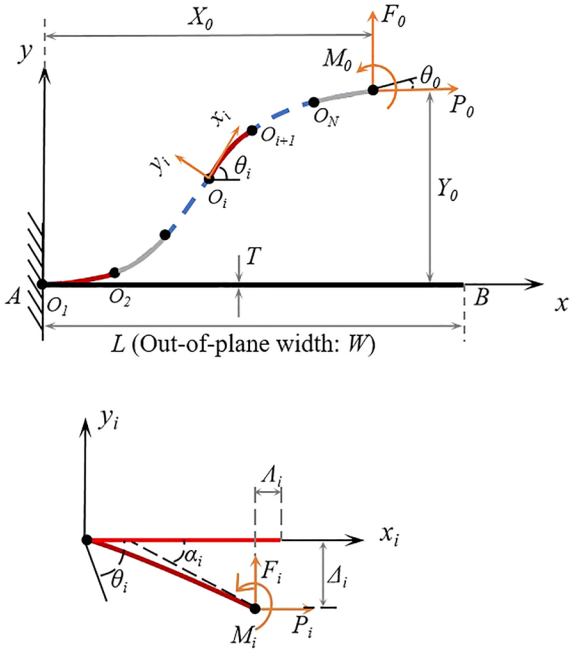

Figure 4 Discretization of the beam

where d is the displacement at the guided end of the beam. The tip slope remains constant during the movement of the beam, which is shown in Figure 4. Suppose that the beam is divided into N elements with equal length. For the ith $(1 \le i \le N)$ element, its local coordinate frame $(O_i x_i y_i)$ is attached to and moves along with the free end of $(i-1)$th element, i.e., node $(i-1)$. Note that the first element was fixed to the ground at node 0 and the free end of the beam is node N. We use P_i, F_i, and M_i to represent the axial force, the transverse force and the end moment applied on the ith element at node i with respect to its local coordinate frame, where Λ_i, Δ_i, and α_i denote the corresponding axial and transverse deflections and the end slope respectively. The discretization introduces $6N$ intermediate parameters of each element, all of which are normalized with respect to the length of an element as:

$$\begin{aligned} p_i &= \frac{P_i L^2}{N^2 EI}, f_i = \frac{F_i L^2}{N^2 EI}, m_i = \frac{M_i L}{NEI}, \\ \lambda_i &= \frac{N\Lambda_i}{L}, \delta_i = \frac{N\Delta_i}{L}, \alpha_i = \alpha_i. \end{aligned} \tag{9}$$

The load-deflection relations of each beam element are expressed as:

$$\begin{aligned} \begin{bmatrix} f_i \\ m_i \end{bmatrix} &= \begin{bmatrix} 12 & -6 \\ -6 & 4 \end{bmatrix} \begin{bmatrix} \delta_i \\ \alpha_i \end{bmatrix} \\ &+ \frac{p_i}{30} \begin{bmatrix} 36 & -3 \\ -3 & 4 \end{bmatrix} \begin{bmatrix} \delta_i \\ \alpha_i \end{bmatrix} \\ &+ \frac{p_i^2}{6300} \begin{bmatrix} -9 & 4.5 \\ 4.5 & -11 \end{bmatrix} \begin{bmatrix} \delta_i \\ \alpha_i \end{bmatrix}, \end{aligned} \tag{10}$$

$$\begin{aligned} \lambda_i = &\frac{t^2 p_i}{12} - \frac{1}{60} \begin{bmatrix} \delta_i & \alpha_i \end{bmatrix} \begin{bmatrix} 36 & -3 \\ -3 & 4 \end{bmatrix} \begin{bmatrix} \delta_i \\ \alpha_i \end{bmatrix} \\ &- \frac{p_i}{6300} \begin{bmatrix} \delta_i & \alpha_i \end{bmatrix} \begin{bmatrix} -9 & 4.5 \\ 4.5 & -11 \end{bmatrix} \begin{bmatrix} \delta_i \\ \alpha_i \end{bmatrix}, \end{aligned} \tag{11}$$

where t is the normalized width of the beam.

Since the fixed-guided compliant beam is divided into N beam elements, we have $3N$ element equations. In this case, static balancing equations need to be supplemented. The static balancing equation of the ith element with respect to its previous element is formulated as follows:

$$\begin{bmatrix} f'_{i-1} \\ p'_{i-1} \\ m'_{i-1} \end{bmatrix} = \begin{bmatrix} 1 & 0 & 0 \\ 0 & 1 & 0 \\ 1+\lambda_i & -\delta_i & 1 \end{bmatrix} \begin{bmatrix} f_i \\ p_i \\ m_i \end{bmatrix}. \tag{12}$$

Because the ith element goes through a rigid body rotation α_{i-1} with the deflection of the $(i-1)$th element, we have

$$\begin{bmatrix} f_{i-1} \\ p_{i-1} \\ m_{i-1} \end{bmatrix} = \begin{bmatrix} \cos\alpha_{i-1} & \sin\alpha_{i-1} & 0 \\ -\sin\alpha_{i-1} & \cos\alpha_{i-1} & 0 \\ 0 & 0 & 1 \end{bmatrix} \begin{bmatrix} f'_{i-1} \\ p'_{i-1} \\ m'_{i-1} \end{bmatrix}. \tag{13}$$

Since the local coordinate frame of the first element coincides with the global coordinate frame of the beam, then we have

$$p_1 = p_o, f_1 = f_o, m_N = m_o. \tag{14}$$

We use θ_i to represent the rotation of the coordinate frame of the ith element relative to the global coordinate frame, thus:

$$\theta_1 = 0, \theta_i = \sum_{k=1}^{i-1} \alpha_k (i = 1, 2, 3, \cdots, N). \tag{15}$$

The static balancing equations between the first beam element and the ith $(2 \le i \le N)$ beam element are written as

$$\begin{bmatrix} \cos\theta_i & \sin\theta_i & 0 \\ -\sin\theta_i & \cos\theta_i & 0 \\ (1+\lambda_i) & -\delta_i & 1 \end{bmatrix} \begin{bmatrix} f_i \\ p_i \\ m_i \end{bmatrix} = \begin{bmatrix} f_1 \\ p_1 \\ m_{i-1} \end{bmatrix}. \tag{16}$$

In addition, there are 3 constraints related to the geometric compatibility for the whole beam:

$$\begin{cases} \sum_{i=1}^{N-1} \left[\begin{bmatrix} \cos\theta_i & -\sin\theta_i \\ \sin\theta_i & \cos\theta_i \end{bmatrix} \begin{bmatrix} L_i(1+\lambda_i) \\ L_i\delta_i \end{bmatrix} \right] = \begin{bmatrix} X_0 \\ Y_0 \end{bmatrix}, \\ \theta_N + \alpha_N = \theta_0. \end{cases} \tag{17}$$

In summary, the CBCM model has $(6N+3)$ equations to accommodate the $6N$ intermediate parameters generated in the discretization. For the six parameters F_o, P_o, M_o, X_o, Y_o, and θ_o at the end of the fixed-guided compliant beam, if the last three are known, the first three can be solved, vice versa. The reaction force F at the guided end of the compliant beam along its moving direction is:

$$F = P_o \cos\theta_o - F_o \sin\theta_o. \tag{18}$$

By substituting the parameters of the fixed-guided compliant beam into the above formula (the beam material is assumed to be 65Mn Spring Steel whose Young's modulus $E = 2.1\times10^{11}$ Pa). To further verify the design results, a finite element model for the constant-force design was established in ABAQUS [18]. The beam was divided into 60 elements, with each element modeled using the B22 element. A gradually increased displacement is applied at the beam tip to observe the change of the output force of the mechanism.

The finite element model successfully captures the rapid increase of the output force at the beginning of deflection followed by an extensive range of constant output force. The finite element results are compared with the results of CBCM in Figure 5. The two curves agree well with each other, with the maximum error less than 5%. The results verify effectiveness of the single compliant beam design.

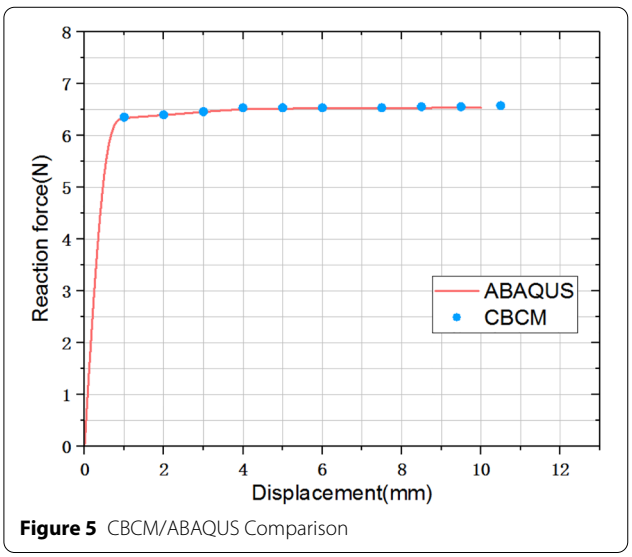

Figure 5 CBCM/ABAQUS Comparison

3 Structure Design of Constant-Force End-Effector

The constant-force end-effector is installed at the end of the industrial robot via a flange. The main functionality of the end-effector is to maintain a constant contact force between the polishing head and the workpiece during the polishing process [19–21]. When the robot adjusts the polishing head according to the polishing trajectory, the end-effector keeps the polishing head in contact with the workpiece. Meanwhile, the end-effector applies a constant force to the workpiece through the deflection of the constant-force compliant mechanism.

As mentioned in the previous section, four compliant beams are utilized and symmetrically arranged for the constant-force end effector to increase its stability. The material of the compliant beams was made of Annealing 65Mn Spring Steel. To eliminate the errors in the movement of the industrial robot in the polishing trajectory, we further add a slide rail for the end-effector to guide the deflection of the compliant beams and eliminate the unexpected vibration. The rotary motion and constant force unit are separated by using a double-row deep groove ball bearing as the transmission mechanism of rotary motion. This way improves operational stability and reduces possible vibration during polishing. The exploded view of the whole end-effector is shown in Figure 6. In addition, a brushless DC motor is employed to drive the polishing head.

The compliant beams in the constant force mechanism are thin and vulnerable to forced vibration that could worsen the constant-force behavior. To improve the overall stability in the work process, the constant-force mechanism doesn't rotate along with the rotation of the polishing head, which is realized by employing a double row deep groove ball bearing between the polishing head and the constant-force mechanism. To guarantee stable relative motion between the polishing head and

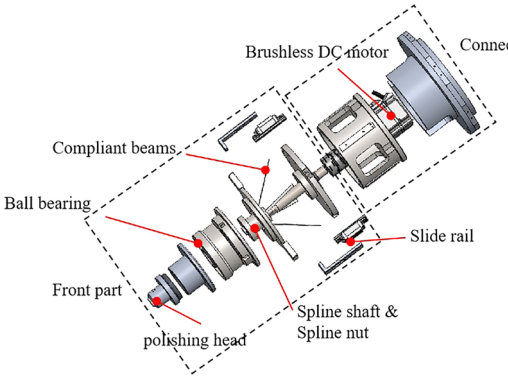

Figure 6 Exploded view of the end-effector

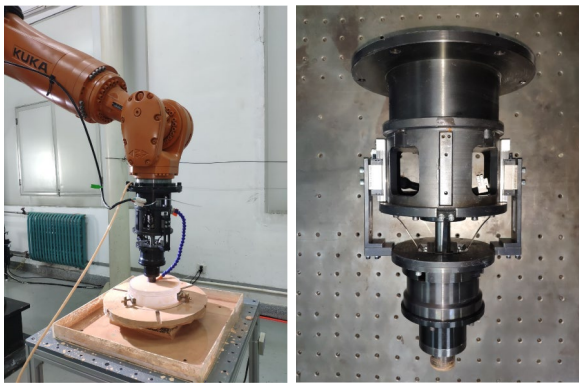

(a) Polishing assembly (b) End-effector

Figure 7 Experimental setup of robotic polishing

the constant-force mechanism, we use two precise slide rails to guide the fixed-guided deflection of the compliant beams and avoid lateral drift. These design details improve operational stability and reduces harmful vibration during polishing.

4 Experiments

To verify the mechanical performance and stability of the constant-force end-effector, two experiments, including a performance-test experiment and a polishing experiment, are presented in this section. A load cell is mounted on the output-end of the end-effector to measure the contact force in the experiments. Figure 7 shows the experimental setup of polishing robot and the constant-force end-effector.

4.1 Performance Test

The performance-test experiment mainly tests the capability of maintaining the constant-force of the constant-force mechanism in the end-effector under static and dynamic conditions. The static contact-force test shows that the constant-force mechanism can output a near-constant force in a large range of displacement along Z direction in both forward and backward movement, with the fluctuation error within 3.08 N, as shown in Figure 8(a).

We tested the constant force fluctuations at different spindle speeds and found out that the fluctuation is relatively lower when the spindle speed is 200 r/min, and the corresponding relationship between force and displacement at 200 r/min is shown in Figure 8(b). This spindle speed was selected for the rest of the experiments. Both the static and dynamic experimental results confirmed that the designed constant-force end-effector achieves the goal of fluctuation error within 5%.

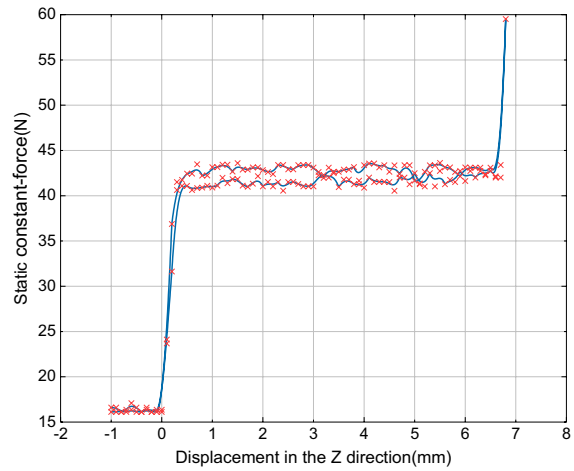

(a) Static performance

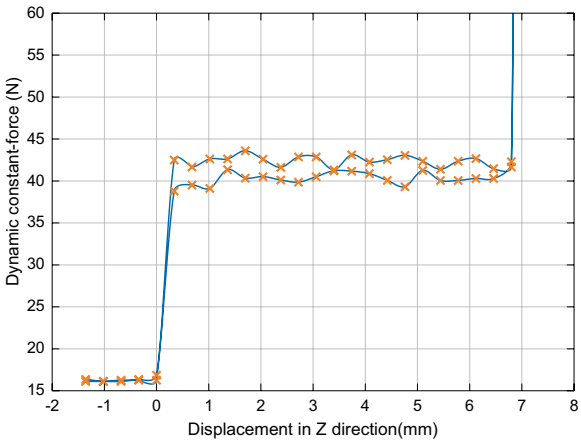

(b) Dynamic performance

Figure 8 Experimental results of the constant force behaviors

A hysteresis between the forward and backward movement of the contact-force end-effector is observed in both static and dynamic experiments. This could be mainly attributed to the friction and the clearance in the guide rails. The hysteresis can be reduced by employing high-quality guide rails but cannot be eliminated.

We also compared the performance of the constant-force end-effector (passive) to that of a pneumatically controlled end-effector (active) developed in our lab. The constant-force end-effector exhibits a much faster response, because each compliant beam generates a constant force immediately after its deflection in the effective deflection range. However, for the pneumatically controlled end-effector, the air cylinder needs relatively longer time to repeatedly inflate or deflate so as to achieve a constant-force output in the nonlinear feedback control. In the multiple measurements, we found that the average response time of the

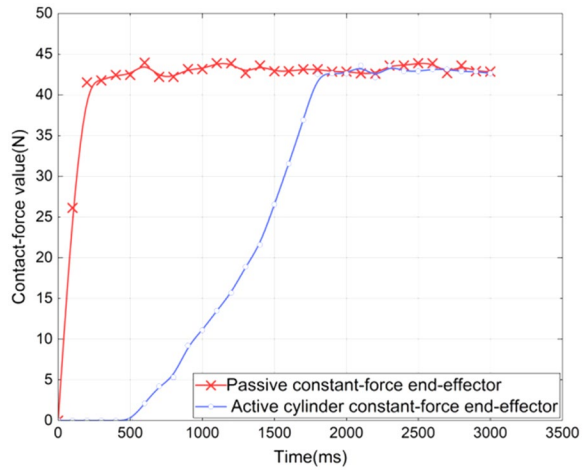

Figure 9 Response time comparison

constant-force end-effector is less than 200 ms, while the average response time of the pneumatically controlled end-effector reaches 1.5 s. The results are shown in Figure 9.

4.2 Polishing Experiment

In the polishing experiment, a K9 spherical mirror with a diameter of 200 mm and a radius of curvature of 467 mm is polished. For optical polishing, the removal function of the end-effector is also essential. The Princeton equation [22, 23] shows that the amount of material removed is positively correlated with relative linear velocity, normal contact force, and scale factor. Based on the Preston equation, the removal function with the shape of an inverted cone shown in Figure 10 is selected to improve the polishing efficiency, with the largest removal amount at the edge and gradually decreased as the polishing head moves to the center.

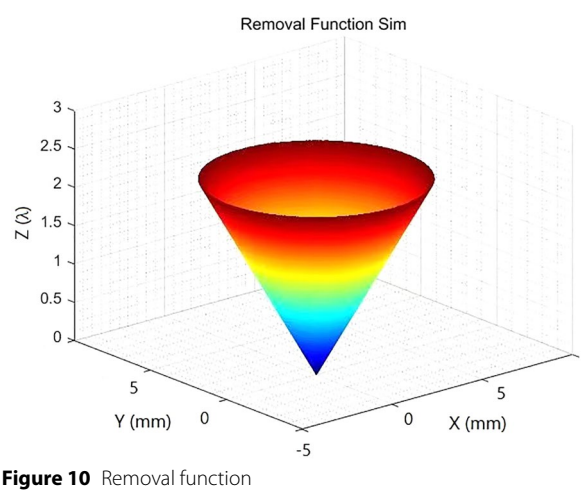

Figure 10 Removal function

It is well known that the traditional grinding trajectory is prone to induce serious edge effects, which is not conducive to precise modification of mirror surfaces [24, 25]. A cycloidal motion along the mirror generatrix is adopted, which can improve the uniformity of the trajectory and reduce the edge effects. That is, the center of the polishing head moves inward along the generatrix starting from the outer edge of the mirror, which revolves with the turntable. The simulated results of the trajectory and the area covered by the polishing head are shown in Figure 11. The trajectory (red line) with the uniform speed motion (pink line) is an equidistant spiral. The area swept per unit time by the polishing head (blue dotted line) decreases as it moves from the edge to the center, while the equivalent retention time increases (Figure 11(a)). The increase of the equivalent retention time will likely induce concave removal on the workpiece. Therefore, a variable speed trajectory is adopted during the polishing process, with which the polishing head of the end-effector accelerates from the outer edge of the mirror to the center along the generatrix, which can counteract the increase of equivalent retention time. As shown in Figure 11(b), the motion of the variable speed generatrix as a non-equidistant spiral, in which the pitch widens as R decreases.

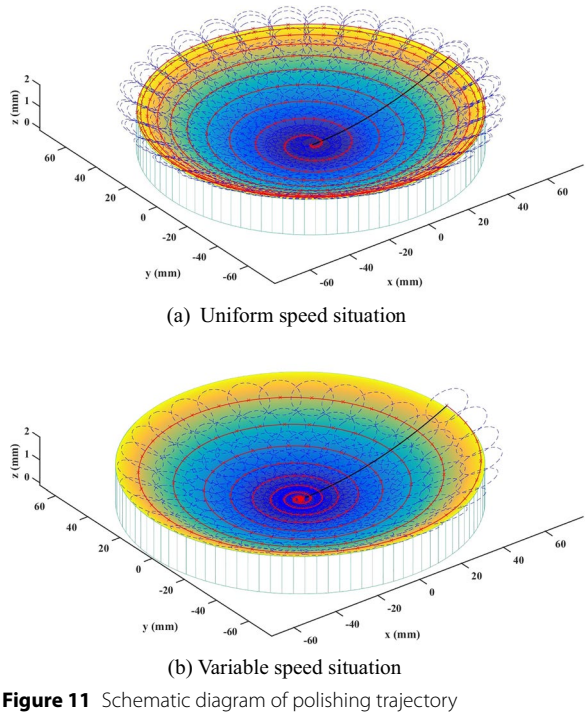

(a) Uniform speed situation

(b) Variable speed situation

Figure 11 Schematic diagram of polishing trajectory

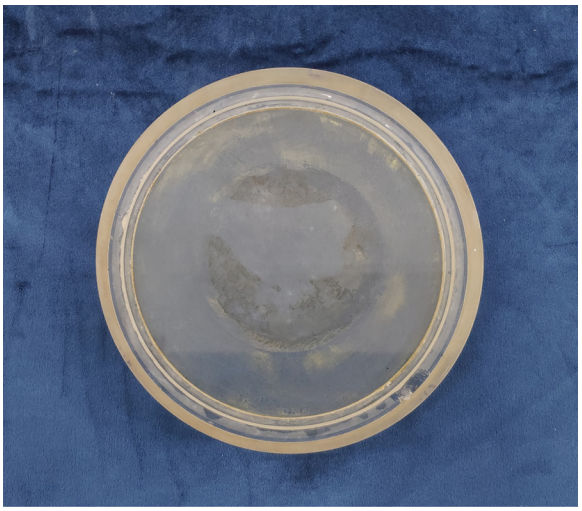

(a) K9 Spherical mirror

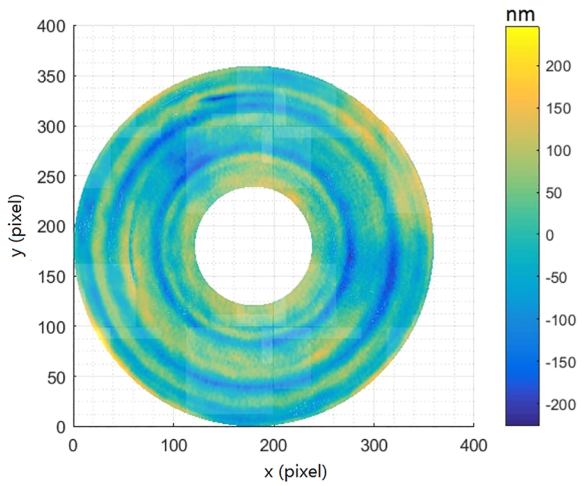

(b) Interferogram result

Figure 12 The result of the polished mirror (the plus and minus signs represent the position relative to *xy*-plane)

The polished K9 spherical mirror is shown in Figure 12(a). In the polishing experiment, the peak removal rate is 2.37 λ/s (≈1.5 μm/s) with spindle speed of 200 r/min and contact force of 40 N, which is consistent with the removal function. The interferogram results shown in Figure 12(b) indicate that the RMS of the polished surface reaches λ/10, which meet our expectations.

5 Conclusions

This paper designed a compliant constant-force mechanism for robotic polishing to passively maintain a constant force between the robot and the workpiece. The use of constant-force mechanism eliminates the requirements of force sensing and real-time control. The design was tested experimentally through various conditions. The polishing experiment conducted on a K9 R467 reflective mirror with a diameter of 200 mm shows that the passive constant-force end-effector provides stable pressure with fluctuation within 3.43 N. The RMS of the polished surface of a large-aperture reflective mirror lower than λ/10. Comparing with the traditional methods using force control, the passive method using a constant-force compliant mechanism provides a low-cost and reliable solution for robotic polishing. Noted that, the low-frequency jitter was observed in the experiment, which could be caused by materials, manufacturing, and assembly issues. Thus, it is necessary to investigate the dynamic behaviors of constant-force end-effector further and improve the polishing performances in later investigation.

Acknowledgements
Not applicable.

Authors' Contributions
JZ and LZ wrote the manuscript; FM and GC proposed design principles and simulation methods; LL carried out corresponding simulations; JZ designed the structure; JZ and LZ carried out experiments and related analyses; All authors read and approved the final manuscript.

Authors' Information
Jian Zhang, born in 1978, is currently a PhD candidate at *School of Mechano-Electrical Engineering, Xidian University, China*. His research interest is robotic polishing of optical reflective mirrors.
Liangxiao Zhao, born in 1993, is currently a PhD candidate at *University of Chinese Academy of Sciences, China*. His research interest is robotic polishing of optical reflective mirrors.
Lingling Li, born in 1997, is currently a master candidate at *Institute of Robotics and Intelligent Systems, Xi'an Jiaotong University, China*. Her research interest is compliant mechanism.
Fulei Ma, born in 1988, is currently a lecture at *School of Mechano-Electrical Engineering, Xidian University, China*. His research interests include compliant mechanisms and their applications in robotics.
Guimin Chen, born in 1978, is a professor and the director of *Institute of Robotics and Intelligent Systems, Xi'an Jiaotong University, China*. His research interests include compliant mechanisms and their applications in robotics.

Funding
Supported by National Natural Science Foundation of China (Grant No. U1913213), West Light Foundation of the Chinese Academy of Sciences (Grant No. XAB2016A10), and Shanxi Provincial Key Research and Development Projects of China (Grant No. 2018ZDXM-GY-105).

Availability of Data and Materials
The datasets supporting the conclusions of this article are included within the article.

Ethics Approval and Consent to Participate
Not applicable.

Consent for Publication
Not applicable.

Competing Interests
The authors declare no competing financial interests.

Author Details
[1]School of Mechano-Electrical Engineering, Xidian University, Xi'an 710071, China. [2]Xi'an Institute of Optics and Precision Mechanics of CAS, Xi'an 710119, China. [3]University of Chinese Academy of Sciences, Beijing 100049, China. [4]Institute of Robotics and Intelligent Systems, Xi'an Jiaotong University, Xi'an 710049, China.

Received: 20 December 2021 Revised: 21 October 2022 Accepted: 26 October 2022
Published online: 24 November 2022

References

[1] L S Tsesnek, V E Guzman, Y N Nasonov, et al. Equipment for the grinding & polishing of optical-components on production liens. *Soviet Journal of Optical Technology*, 1981, 48(10): 623-632.
[2] R K Pal, H Garg, V Karar. Material removal characteristics of full aperture optical polishing process. *Machining Science and Technology*, 2017, 21(4): 493-525.
[3] X Wu, Z Huang, Y J Wan, et al. A novel force-controlled spherical polishing tool combined with self-rotation and co-rotation motion. *IEEE Access*, 2020, 8: 108191-108200.
[4] X D Zhang, H Chen, N Yang, et al. A structure and control design of constant force polishing end actuator based on polishing robot. *2017 IEEE International Conference on Information and Automation (IEEE ICIA 2017),* 2017: 764-768.
[5] S Moriyasu, C Liu, W Lin, et al. Development of ultra-precision constant pressure spindle head for aspherical grinding/polishing. In: *Progress of machine technology.* Aviation Industry Press, 2002: 494-497.
[6] D H Su, X Liu. The simulation and study of buffer device of hydraulic cylinder. In: *Advanced materials research*. Trans. Tech. Publications Ltd., 2012, (591): 561-564.
[7] X D Zhang, H Chen, N Yang, et al. A structure and control design of constant force polishing end actuator based on polishing robot. *2017 IEEE International Conference on Information and Automation*, 2017: 764-768.
[8] D Bossert, U Ly, J Vagners. Experimental evaluation of a hybrid position and force surface following algorithm for unknown surfaces. *IEEE International Conference on Robotics and Automation*, Minneapolis, 1996: 22-28.
[9] L L Howell. *Compliant mechanisms*. New York: Wiley, 2001.
[10] D L Blanding. *Exact constraint: machine design using kinematic processing.* New York: ASME, 1999.
[11] Y Chen, C Lan. An adjustable constant-force mechanism for adaptive end-effector operations. *Journal of Mechanical Design*, 2012,134(3): 031005.
[12] G Chen, S Zhang. Fully-compliant statically-balanced mechanisms without prestressing assembly: concepts and case studies. *Mechanical Science*, 2011, 2(2): 169-174.
[13] G Chen, Y Gou, A Zhang. Synthesis of compliant multistable mechanisms through use of a single bistable mechanism. *Journal of Mechanical Design*, 2011, 133(8): 081007.
[14] Y Kuo, C Lan. A two-dimensional adjustable constant-force mechanism. *Journal of Mechanical Design,* 2020,142(6): 063304.
[15] F Ma, G Chen. Large-stroke constant-force mechanisms utilizing second buckling mode of flexible beams: evaluation metrics and design approach. *Journal of Mechanical Design*, 2020,142(10): 103303.
[16] F Ma, G Chen. Modeling large planar deflections of flexible beams in compliant mechanisms using chained beam-constraint-model. *Journal of Mechanisms and Robotics*, 2016, 8(2).
[17] G Chen, F Ma, G Hao, et al. Modeling large deflections of initially curved beams in compliant mechanisms using chained beam-constraint-model. *Journal of Mechanisms and Robotics*, 2019, 11(1).
[18] S Zhuang, F Zhang, L Song. *ABAQUS nonlinear finite element analysis and examples*. Beijing: Science Press, 2005.
[19] M A F Lora, E A Portilla-Flores, R R Blas, et al. Metaheuristic techniques comparison to optimize robotic end-effector behavior and its workspace. *International Journal of Advanced Robotics Systems,* 2018, 15(5).
[20] A Mohammad, J Hong, D W Wang. Design of a force-controlled end-effector with low-inertia effect for robotic polishing using macro-mini robot approach. *Robotics and Computer-Integrated Manufacturing*, 2018, 49: 54-65.
[21] Y S Yao, Z Ma, J T Ding, et al. Heavy-calibre off-axis aspheric surface polishing by industrial robot. *9th International Symposium on Advanced Optical Manufacturing and Testing Technologies,* 2019, 10838.
[22] X Wang, X J Zhang. Theoretical study on removal rate and surface roughness in grinding a RB-SiC mirror with a fixed abrasive. *Applied Optics,* 2009, 48(5): 904-910.
[23] Z Xia, F Fang, Ahearne E, et al. Advances in polishing of optical freeform surfaces: A review. *Journal of Materials Processing Technology*, 2020, 286: 116828.
[24] W Song, X Zhang, M Xu. Region-adaptive path planning for precision optical polishing with industrial robots. *Optical Express*, 2018, 26(10): 23782-23794.
[25] W L Zhu, A Beaucamp. Zernike mapping of optimum dwell time in deterministic fabrication of freeform optics. *Optical Express*, 2019, 27(20): 28692-28706.